DESIGN, SYNTHESIS, BIOLOGICAL EVALUATION, AND MOLECULAR DOCKING STUDIES OF *ORTHO*-CARBOXAMIDO STILBENES AS ANTI-DIABETIC AND ANTI-PROLIFERATIVE AGENTS

NORHADI BIN MOHAMAD

UNIVERSITI SAINS MALAYSIA

2022

DESIGN, SYNTHESIS, BIOLOGICAL EVALUATION, AND MOLECULAR DOCKING STUDIES OF *ORTHO*-CARBOXAMIDO STILBENES AS ANTI-DIABETIC AND ANTI-PROLIFERATIVE AGENTS

by

NORHADI BIN MOHAMAD

Thesis submitted in fulfilment of the requirements
for the degree of
Master of Science

September 2022

ACKNOWLEDGEMENT

In the name of Allah, the Most Gracious and the Most Merciful.

I would like to convey my utmost gratitude to my main supervisor, Dr. Mohamad Nurul Azmi Mohamad Taib, for his guidance, comments, concern, understanding, and unwavering support throughout the development of this project. I would like to thank my co-supervisors, Dr. Mohamad Hafizi Abu Bakar and Dr. Mohammad Tasyriq Che Omar, for their assistance, guidance, and advice in accomplishing this project. My appreciation extends to Dr. Nik Nur Syazni Nik Mohammad Kamal for the anti-proliferative assay screening from Advanced Medical and Dental Institute (AMDI), USM and Prof. Unang Supratman from Universitas Padjadjaran in HRMS assistance.

I wish to take this opportunity to thank Universiti Sains Malaysia (USM) and the School of Chemical Sciences for all the facilities and assistance throughout my studies. My most profound appreciation is also dedicated to all the science officers at the School of Chemical Sciences for their constant help and patience to guide me to finish my research study.

A special dedication to my dear parents, the pillars of support, and love in my life, for their countless support and blessings to finish my journey in Master of Science (Chemistry). Studying when you are holding a full-time job is demanding and even daunting. I consider myself fortunate because I have always managed to wriggle my way around. Thus, I would like to extend my utmost appreciation to Datin Dr. Annie Foo, my former Head of Department, and my Foundation Department family at RCSI & UCD Malaysia Campus for the encouragement and continuous support that I have received. Finally, I would like to thank my NPSO research team and friends who helped and encouraged me during my research days.

TABLE OF CONTENTS

ACKNOWLEDGEMENT ..... **ii**

TABLE OF CONTENTS ..... **iii**

LIST OF TABLES ..... **viii**

LIST OF FIGURES ..... **ix**

LIST OF SCHEMES ..... **xiii**

LIST OF SYMBOLS ..... **xiv**

LIST OF ABBREVIATIONS ..... **xvi**

LIST OF APPENDICES ..... **xx**

ABSTRAK ..... **xxiii**

ABSTRACT ..... **xxv**

CHAPTER 1 INTRODUCTION **1**

1.1 Overview 1

1.2 Problem Statement 3

1.3 Research Objectives 5

1.4 Scope of Research 5

CHAPTER 2 LITERATURE REVIEW **6**

2.1 Stilbene Compound 6

2.2 Stilbene Synthesis 9

2.3 Role of Stilbenes in the Prevention of Cancer 13

2.3.1 Tubulin protein in cancer 18

2.4 Role of stilbene as enzyme inhibitors of hyperglycemic enzymes and the enzymatic pathways 22

2.4.1 Overview of Diabetes Mellitus (DM) 23

2.4.2 Target protein for diabetes 24

2.4.3 Mechanism of action (MOA) of enzyme 25

2.4.3(a) Competitive inhibition 26
2.4.3(b) Noncompetitive inhibition 28
2.4.3(c) Uncompetitive inhibition 30
2.5 Molecular Docking 32
2.5.1 Database for receptor and ligand 32
2.5.2 Docking software 34
2.5.2(a) Chimera 35
2.5.2(b) AutoDock Vina 35
2.5.2(c) BIOVIA Discovery Studio Visualizer 36
2.6 Current Research Focus 37
CHAPTER 3 METHODOLOGY 38
3.1 Overview 38
3.2 Reagents Used in the Synthesis Work 41
3.3 General Experimental Methods and Instrumentals 41
3.3.1 Melting point 41
3.3.2 Thin layer chromatography (TLC) 42
3.3.3 Column Chromatography (CC) 42
3.3.4 Detector reagents 42
3.3.5 Moisture sensitive reactions 43
3.3.6 Fourier transform infrared (FT-IR) spectroscopy 43
3.3.7 Nuclear magnetic resonance (NMR) spectroscopy 43
3.3.8 High-resolution mass spectrometry (HRMS) elemental analysis 44
3.4 Synthesis Method 45
3.4.1 Preparation of 3,5-dimethoxystyrene (**46**) 46
3.4.2 General procedure for the preparation of *N*-(2-iodophenyl)acrylamides (**49a-49k**) 47
3.4.2(a) *N*-(2-iodophenyl) furan-2-carboxamide (**49a**) 47

3.4.2(b) *N*-(2-iodophenyl)acetamide (**49b**) 48

3.4.2(c) *N*-(2-iodophenyl)-2-bromobenzamide (**49c**) 48

3.4.2(d) *N*-(2-iodophenyl)-4-bromobenzamide (**49d**) 49

3.4.2(e) *N*-(2-iodophenyl)isobutyramide (**49e**) 49

3.4.2(f) *N*-(2-iodophenyl)hexanamide (**49f**) 50

3.4.2(g) *N*-(2-iodophenyl)pentanamide (**49g**) 50

3.4.2(h) *N*-(2-idophenyl)butyramide (**49h**) 51

3.4.2(i) *N*-(2-iodophenyl)benzamide (**49i**) 52

3.4.2(j) *N*-(2-iodophenyl)cyclohexanecarboxamide (**49j**) 52

3.4.2(k) *N*-(2-iodophenyl)-2-methylbenzamide (**49k**) 53

3.4.3 General procedure for the preparation of *ortho*-carboxamido stilbenes (**50a-50k**) 54

3.4.3(a) (*E*)-*N*-(2-(3,5-dimethoxystyryl)phenyl)furan-2-carboxamide (**50a**) 55

3.4.3(b) (*E*)-*N*-(2-(3,5-dimethoxystyryl)phenyl)acetamide (**50b**) 56

3.4.3(c) (*E*)-2-bromo-*N*-(2-(3,5-dimethoxystyryl)phenyl) benzamide (**50c**) 57

3.4.3(d) (*E*)-4-bromo-*N*-(2-(3,5-dimethoxystyryl)phenyl) benzamide (**50d**) 58

3.4.3(e) (*E*)-*N*-(2-(3,5-dimethoxystyryl)phenyl) isobutyramide (**50e**) 59

3.4.3(f) (*E*)-*N*-(2-(3,5-dimethoxystyryl)phenyl)hexanamide (**50f**) 60

3.4.3(g) (*E*)-*N*-(2-(3,5-dimethoxylstyryl)phenyl)pentanamide (**50g**) 61

3.4.3(h) (*E*)-*N*-(2-(3,5-dimethoxystyryl)phenyl)butyramide (**50h**) 62

3.4.3(i) (*E*)-*N*-(2-(3,5-dimethoxystyryl)phenyl)benzamide (**50i**) 63

3.4.3(j) (*E*)-*N*-(2-(3,5-dimethoxystyryl)phenyl) cyclohexanecarboxamide (**50j**) 64

3.4.3(k) (*E*)-*N*-(2-(3,5-dimethoxystyryl)phenyl)-2-methylbenzamide (**50k**) 65

3.5 Anti-Proliferative Assay 66

3.5.1 Cell culturing 66

3.5.2 Cell proliferation assay 66

3.5.3 Selectivity index (SI) 67

3.5.4 Statistical analysis 67

3.6 α-amylase and α-glucosidase Inhibitory Potential of Stilbene (**50a–50e**) 68

3.6.1 Assay for α-amylase inhibition 68

3.6.2 Assay for α-glucosidase inhibition 69

3.6.3 Mode of inhibition of α-amylase 70

3.6.4 Mode of inhibition of α-glucosidase 71

3.6.5 2,2-diphenyl-1-picryl-hydrazyl-hydrate (DPPH) free radical scavenging activity 72

3.6.6 Ferric reducing antioxidant power (FRAP) assay 72

3.6.7 Cell viability assay 73

3.7 Molecular Docking 75

3.7.1 Bioinformatics tool used in molecular docking 75

3.7.2 Ligand preparation 75

3.7.3 Protein preparation 76

3.7.4 Protein-ligand docking 78

3.7.5 Analysis and visualization 82

3.7.6 Validation of Docking Parameters 83

CHAPTER 4 RESULTS AND DISCUSSION 84

4.1 Overview 84

4.2 Towards synthesis of stilbene. 84

4.2.1 Structure elucidation on 3,5-dimethoxystyrene (**46**) 84

4.2.2 Structure elucidation of *N*-(2-iodophenyl)acylamides (**49a-49k**) 88

4.2.3 Structure elucidation of *ortho*-carboxamido stilbene (**50a-50k**) 92

4.2.4 Mechanistic interpretation of results for the Heck coupling reaction 98

4.3 Anti-Proliferative Study 100

4.3.1 Cytotoxic effect of the synthesized compounds on cancer cells lines 101

4.3.2 Molecular docking study 108

4.4 Anti-diabetic Studies 113

4.4.1 α-amylase and α-glucosidase inhibitory assays 113

4.4.2 Mode of α-amylase and α-glucosidase inhibitions 114

4.4.3 Antioxidant assay 117

4.4.4 *In vitro* cell viability assay 119

4.4.5 Molecular docking study 121

4.5 The Structure-activity Relationship (SAR) Studies 128

4.5.1 SAR for anti-proliferative studies 129

4.5.2 SAR for anti-diabetic studies 129

CHAPTER 5 CONCLUSION AND RECOMMENDATIONS 131

5.1 Conclusion 131

5.2 Recommendations for Future Research 133

REFERENCES 134

APPENDICES

LIST OF PUBLICATIONS

LIST OF TABLES

Page

Table 3.1 Protein PDBs and Biological Studies.....77

Table 3.2 Protein PDB with respective 2D and 3D compound structures 79

Table 3.3 The grid boxes (x, y, and z at 0.375 Å spacing) used to perform docking for each protein receptor 81

Table 4.1 The physical properties of *N*-(2-iodophenyl)acylamides (**49a–49k**) 88

Table 4.2 The physical properties of *ortho*-carboxamido stilbene (**50**).....93

Table 4.3 Classification of anti-proliferative activities based on the IC_{50} values.....100

Table 4.4 The *o*-carboxamido stilbenes analogs (**50**) and their correlated IC_{50} values and selective index (SI) on cancer cell lines.....104

Table 4.5 *In-silico* binding energy between compounds (**50d**), **(50f**), and (**50g**) with either α-tubulin or *β*-tubulin subunit 108

Table 4.6 Binding interactions between active compounds with either α-tubulin or *β*-tubulin subunit.....111

Table 4.7 IC_{50} values for α-amylase and α-glucosidase inhibitory for compounds (**50a–50e**).....114

Table 4.8 IC_{50} values for DPPH free radical scavenging activity of compound (**50a-50e**) 118

Table 4.9 FRAP values for of the compounds (**50a-50e**) 119

Table 4.10 *In-silico* binding energy between compound (**50a–50e**) with either α-amylase or α-glucosidase (ctMGAM) 121

Table 4.11 Binding interactions between active compounds (**50b-50e**) with either α-amylase or α-glucosidase (ctMGAM) 126

Table 4.12 Substitution pattern of the R groups of amides.....128

LIST OF FIGURES

Page

Figure 1.1 The chemical structures of stilbenes isomers.....1

Figure 1.2 The chemical structures of *trans*-polyphenolic stilbenes.....2

Figure 1.3 The bar chart of Global Health Estimates 2019 (World Health Organization, 2020).....4

Figure 2.1 Some examples of plant polyphenols.....6

Figure 2.2 Structure of compound (**19)** 10

Figure 2.3 Structure of compound (**23**) 11

Figure 2.4 Structure of compound (**28**) 13

Figure 2.5 Structure of compound (**29**) 14

Figure 2.6 Structure of compound (**30**) 15

Figure 2.7 Structure of 4-methylsubstituted *trans*-stilbene with significant inhibitory action toward three cancer cell lines 15

Figure 2.8 Structure of amide substituted resveratrol with potent cytotoxicity towards the respective cancer cell lines 16

Figure 2.9 Structure of modified stilbene (**39**) with the most proficient anti-cervical cancer agent with the self-aggregation property 18

Figure 2.10 Structure of tubulin dimer and its cross-section.....19

Figure 2.11 Structure of Combretastatin A-4 (CA-4).....20

Figure 2.12 Structure of compound (**41**) 20

Figure 2.13 Structure of compound (**42)** 21

Figure 2.14 Structure of compound (**43**) 22

Figure 2.15 Structure of compound (**44**) 23

Figure 2.16 Examples Illustrations of data demonstrating Competitive, Noncompetitive, and Uncompetitive Inhibition (Strelow et al., 2004) 26

Figure 2.17 Examples of Competitive Inhibition where Substrate (S) and Inhibitor (I) binding events are mutually exclusive. 27

Figure 2.18 Graphical representation of competitive inhibition (Yadav & Magadum, 2017) 28

Figure 2.19 Examples of Noncompetitive Inhibition in which Inhibitor (I) binds to a site distinct from the Substrate (S) binding site and the Catalytic center (c) of the active site. 29

Figure 2.20 Double reciprocal plot of noncompetitive inhibition (Yadav & Magadum, 2017) 30

Figure 2.21 Examples Uncompetitive Inhibition where Inhibitor (I) only binds in the presence of Substrate (S) (Strelow et al., 2004) 30

Figure 2.22 Graphical representation of uncompetitive inhibition (Yadav & Magadum, 2017) 31

Figure 2.23 Ligand/Compound 3D structure was built from ChemDraw Ultra 2.0 33

Figure 2.24 Protein Data Bank (PDB) homepage 34

Figure 2.25 Protein-Ligand Docking steps 35

Figure 3.1 Research workflow of design, synthesis, biological evaluation, and molecular docking studies of *ortho*-carboxamido stilbenes as anti-diabetic and anti-proliferative agent 40

Figure 3.2 *In vitro* anti-diabetic studies of stilbene (**50a–50e**) 68

Figure 3.3 3D Structure of compound (**50d**) in Chem3D application (version 13.0). 76

Figure 3.4 PDB ID: 5LYJ was fetched using UCSF Chimera (version 1.14) 77

Figure 3.5 Processed Chain B of 5LYJ (β-Tubulin) with removed water and all non-standard molecules or ions 78

Figure 3.6 Receptor and ligand options configuration in AutoDock Vina.....81

Figure 3.7 Docking result between (**50g**) and α-tubulin.....82

Figure 3.8 Discovery Studio Visualizer window.....83

Figure 4.1 FTIR spectrum of (**46**) 86

Figure 4.2 ^{1}H NMR spectrum ($CDCl_3$, 500 MHz) of (**46**) 86

Figure 4.3 ^{13}C NMR spectrum ($CDCl_3$, 125 MHz) of (**46**) 87

Figure 4.4 FTIR spectrum of (**49e**).....90

Figure 4.5 ^{1}H NMR spectrum ($CDCl_3$, 500 MHz) of (**49e**) 91

Figure 4.6 ^{13}C NMR spectrum ($CDCl_3$, 125 MHz) of (**49e**) 91

Figure 4.7 FTIR spectrum of (**50e**).....95

Figure 4.8 ^{1}H NMR spectrum ($CDCl_3$, 500 MHz) of (**50e**) 96

Figure 4.9 ^{13}C NMR spectrum ($CDCl_3$, 125 MHz) of (**50e**) 96

Figure 4.10 HRMSTOF, HRMS (+ESI) $[M+H]^+$ for (**50e**).....97

Figure 4.11 Two-dimensional binding modes of compound (**50g**) present at active site of α-tubulin.....109

Figure 4.12 Two-dimensional binding modes of compound (**50g**) present at active site of β-tubulin.....110

Figure 4.13 Michaelis-Menten plot for mode of inhibition of α-amylase by (**50e**) 115

Figure 4.14 Lineweaver-Burk plot for the mode of inhibition of α-amylase by (**50e**) 115

Figure 4.15 Michaelis-Menten plot for mode of inhibition of α-glucosidase by (**50d**).....116

Figure 4.16 Lineweaver-Burk plot for mode of inhibition of α-glucosidase by (**50d**).....117

Figure 4.17 Percentage (%) cell viability of MTT assay for (**50d**) at different concentrations 120

Figure 4.18 Percentage (%) cell viability of MTT assay for (**50e**) at different concentrations 120

Figure 4.19 Two-dimensional binding modes of compound (**50d**) present at the active site of C-terminal of human MGAM 122

Figure 4.20 Two-dimensional binding modes of compound (**50c**) present at the active site of C-terminal of human MGAM 123

Figure 4.21 Two-dimensional binding modes of compound (**50e**) present at the active site of α-amylase 124

Figure 4.22 Two-dimensional binding modes of compound (**50b**) present at the active site of α-amylase 125

Figure 4.23 The parent structure of *trans*-stilbene (**50**) 128

LIST OF SCHEMES

Page

Scheme 2.1 Biosynthesis of resveratrol via phenylalanine (Shrestha et al., 2019) 8

Scheme 2.2 General scheme for Heck reaction 9

Scheme 2.3 Synthesis of stilbene (**1**) from Heck reaction 10

Scheme 2.4 Heck–Mizoroki coupling of an aryl halide (**20**) with styrene (**21**) in the presence of catalyst [Gmim]Cl–Pd (II) and Et_3N as a base 11

Scheme 2.5 Heck reaction of aryl bromides with styrene in the presence of K_2CO_3 base and TBAB 12

Scheme 2.6 Synthesis of *trans*-stilbene C-glycosides (**27**) by a microwave-assisted Heck reaction 12

Scheme 2.7 Structure of two stilbene derivatives (**37**) and (**38**) that showed potent antiproliferative activity on U937 cancer cell line 17

Scheme 3.1 The synthesis of *o*-carboxamido stilbenes (**50a–50k**) via the Heck coupling reaction 45

Scheme 4.1 The synthesis of 3,5-dimethoxystyrene (**46**) 84

Scheme 4.2 The synthesis of *N*-(2-iodophenyl)acylamides (**49**) 88

Scheme 4.3 The synthesis of *o*-carboxamido stilbenes (**50**) 92

Scheme 4.4 Plausible mechanism of Heck coupling reaction towards the synthesis of stilbene (**50**) 99

LIST OF SYMBOLS

α	Alpha
Å	Angstrom
Ar	Aryl substituent group
β	Beta
^{13}C NMR	13-Carbon NMR
cm	Centimetre
cm^{-1}	Per centimetre
δ	Chemical shift
δ_C	Chemical shift carbon
δ_H	Chemical shift proton
°C	Degree Celsius
g	Gram
$gmol^{-1}$	Gram per mol
H	Hydrogen atom
Hz	Hertz
I	Iodine atom
J	Coupling constant (Hz)
L	Litre
µM	Micromolar
M	Molarity
m-	Meta
mg	Milligram
MHz	Mega hertz

mL	Millilitre
mm	Millimetre
mm^2	Square millimetre
mmol	Millimol
nM	Nanomolar
o-	*Ortho*
p-	*Para*
ppb	Parts per billion
ppm	Parts per million
%	Percentage
% T	Percentage transmittance
%Yield	Percentage yield
^{1}H-NMR	Proton NMR
R	Alkyl Substituent group

LIST OF ABBREVIATIONS

A549	Human lung epithelial cancer cell line
Akt	Protein kinase B
b.p	Boiling point
BHK-21	Baby Hamster Kidney cell line
BT-549	Human breast cancer cell line
Bu_3N	Tributylamine
BxPC-3	Human pancreatic cancer cell line
$BMIMBF_4$	1-Butyl-3-methylimidazolium tetrafluoroborate
$BMIMBF_6$	1-Butyl-3-methylimidazolium hexafluorophosphate
cat.	Catalyst
CC	Column chromatography
$CDCl_3$-d_1/$CDCl_3$	Deuterated chloroform
COSY	^1H-^1H correlation spectroscopy
CoA	coenzyme A
Cu(II)	Copper (II)
CYPIA1	Cytochrome P450- Family 1 Subfamily A Member 1
CYPIA2	Cytochrome P450- Family 1 Subfamily A Member 2
CYPIB1	Cytochrome P450- Family 1 Subfamily B Member 1
DEPT	Distortionless enhancement by polarization transfer
d	Doublet
dd	Doublet of doublets
DCM	Dichloromethane
DMF	Dimethylformamide

DMEM	Dulbecco's Modified Eagle's Medium
DMSO	Dimethyl sulfoxide
DNA	Deoxyribonucleic acid
DNS	Dinitrosalicyclic acid
dt	Doublet of triplets
DU-145	Human prostate cancer cell lines
DPPH	2, 2-diphenyl-1-picrylhydrazyl
Equiv.	Equivalent
Et_3N	Triethylamine
EtOAc	Ethyl acetate
FTIR	Fourier transform infrared
FBS	Fetal bovine serum
FRAP	Ferric reducing antioxidant power
G2/M	Gap 2/Mitosis phase
GI_{50}	Growth inhibitory at 50 %
H460	Human lung cancer cell line
HT-29	Human colon cancer cell line
hTERT-HPNE	Human pancreatic nestin expressing cells
hEGF	Recombinant human epidermal growth factor
H_2O	Water
HI	Hydrogen iodide
HRMS	High resolution mass spectrometry
hr	Hour(s)
IC_{50}	Inhibition concentration at 50 %
IC_{10}	Inhibition concentration at 10 %

IC_{25}	Inhibition concentration at 25 %
IR	Infrared
JR8	Human melanoma cancer cell line
Jurkat	Human T lymphocyte cancer cell line
K_2CO_3	Potassium carbonate
KI	Potassium iodide
LDL	Low density lipoprotein
m	Multiplet
MCF-7	Human estrogen receptor-positive breast cancer cell line
MDA-MB-231	Human estrogen receptor-negative breast cancer cell line
min	Minute(s)
MW	Microwave
MYB-14	(a TT2 homolog) in the model legume *Medicago truncatula*
$NaH_2PO_4.2H_2O$	Sodium phosphate monobasic dihydrate
NH_4Cl	Ammonium chloride
NaOH	Sodium hydroxide
NCDs	Non-communicable diseases
n.d	Not determined
NMR	Nuclear magnetic resonance
Na_2CO_3	Sodium carbonate
Pd	Palladium
PDB	Protein data bank
PenStrep	Penicillin-streptomycin
$PdCl_2$	Palladium dichloride
$Pd(OAc)_2$	Palladium (II) acetate

P388	Leukemia cells
pNPG	*p*-nitrophenyl glucopyraboside
QR2	Quinone reductase 2 enzyme
RAW 264.7	Murine monocytic cells
RS	Relative survival
s	Singlet
SAR	Structure-activity relationship
t	Triplet
TBAB	Tetrabutylammonium bromide
TBAE	2-[(1,1-dimethylethyl)amino]ethanol
td	Triplet of doublets
TEA	Triethanolamine
THF	Tetrahydrofuran
TLC	Thin layer chromatography
TMS	Tetramethylsilane
TPTZ	2,4,6-Tris(2-pyridyl)-s-trizaine
UV	Ultraviolet
U937	Histiocytic Lymphoma; Human (Homo sapiens)
WRL-68	Human hepatic cancer cell line

LIST OF APPENDICES

Appendix 1 ^{1}H NMR spectrum for compound (**50a**) in $CDCl_3$ at 500 MHz

Appendix 2 ^{13}C NMR spectrum for compound (**50a**) in $CDCl_3$ at 125 MHz

Appendix 3 ^{1}H NMR spectrum for compound (**50b**) in $CDCl_3$ at 500 MHz

Appendix 4 ^{13}C NMR spectrum for compound (**50b**) in $CDCl_3$ at 125 MHz

Appendix 5 ^{1}H NMR spectrum for compound (**50c**) in $CDCl_3$ at 500 MHz

Appendix 6 ^{13}C NMR spectrum for compound (**50c**) in $CDCl_3$ at 125 MHz

Appendix 7 ^{1}H NMR spectrum for compound (**50d**) in $CDCl_3$ at 500 MHz

Appendix 8 ^{13}C NMR spectrum for compound (**50d**) in $CDCl_3$ at 125 MHz

Appendix 9 ^{1}H NMR spectrum for compound (**50f**) in $CDCl_3$ at 500 MHz

Appendix 10 ^{13}C NMR spectrum for compound (**50f**) in $CDCl_3$ at 125 MHz

Appendix 11 ^{1}H NMR spectrum for compound (**50g**) in $CDCl_3$ at 500 MHz

Appendix 12 ^{13}C NMR spectrum for compound (**50g**) in $CDCl_3$ at 125 MHz

Appendix 13 ^{1}H NMR spectrum for compound (**50h**) in $CDCl_3$ at 500 MHz

Appendix 14 ^{13}C NMR spectrum for compound (**50h**) in $CDCl_3$ at 125 MHz

Appendix 15 ^{1}H NMR spectrum for compound (**50i**) in $CDCl_3$ at 500 MHz

Appendix 16 ^{13}C NMR spectrum for compound (**50i**) in $CDCl_3$ at 125 MHz

Appendix 17 ^{1}H NMR spectrum for compound (**50j**) in $CDCl_3$ at 500 MHz

Appendix 18 ^{13}C NMR spectrum for compound (**50j**) in $CDCl_3$ at 125 MHz

Appendix 19 ^{1}H NMR spectrum for compound (**50k**) in $CDCl_3$ at 500 MHz

Appendix 20 ^{13}C NMR spectrum for compound (**50k**) in $CDCl_3$ at 125 MHz

Appendix 21 HRMSTOF, HRMS (+ESI) $[M+Na]^+$ for compound (**50a**)

Appendix 22 HRMSTOF, HRMS (+ESI) $[M+Na]^+$ for compound (**50b**)

Appendix 23 HRMSTOF, HRMS (+ESI) [M+H]- for compound (**50c**)

Appendix 24 HRMSTOF, HRMS (+ESI) $[M+H]^-$ for compound (**50d**)

Appendix 25 HRMSTOF, HRMS (+ESI) $[M+H]^+$ for compound (**50f**)

Appendix 26 HRMSTOF, HRMS (+ESI) $[M+H]^+$ for compound (**50g**)

Appendix 27 HRMSTOF, HRMS (+ESI) $[M+H]^+$ for compound (**50h**)

Appendix 28 HRMSTOF, HRMS (+ESI) $[M+H]^+$ for compound (**50i**)

Appendix 29 HRMSTOF, HRMS (+ESI) $[M+H]^+$ for compound (**50j**)

Appendix 30 HRMSTOF, HRMS (+ESI) $[M+H]^+$ for compound (**50k**)

Appendix 31 Three-dimensional (above) and two-dimensional (below) binding modes of compound (**50d**) present at active site of α-tubulin

Appendix 32 Three-dimensional (above) and two-dimensional (below) binding modes of compound (**50d**) present at active site of *β*-tubulin

Appendix 33 Three-dimensional (above) and two-dimensional (below) binding modes of compound (**50f**) present at active site of α-tubulin

Appendix 34 Three-dimensional (above) and two-dimensional (below) binding modes of compound (**50f**) present at active site of *β*-tubulin

Appendix 35 Three-dimensional (above) and two-dimensional (below) binding modes of compound (**50g**) present at active site of α-tubulin

Appendix 36 Three-dimensional (above) and two-dimensional (below) binding modes of compound (**50g**) present at active site of *β*-tubulin

Appendix 37 Three-dimensional (above) and two-dimensional (below) binding modes of compound (**50a**) present at active site of α-amylase

Appendix 38 Three-dimensional (above) and two-dimensional (below) binding modes of compound (**50b**) present at active site of α-amylase

Appendix 39 Three-dimensional (above) and two-dimensional (below) binding modes of compound (**50c**) present at active site of α-amylase

Appendix 40 Three-dimensional (above) and two-dimensional (below) binding modes of compound (**50d**) present present at active site of α-amylase

Appendix 41 Three-dimensional (above) and two-dimensional (below) binding modes of compound (**50e**) present at active site of α-amylase

Appendix 42 Three-dimensional (above) and two-dimensional (below) binding modes of compound (**50a**) present at active site of C-terminal of human MGAM

Appendix 43 Three-dimensional (above) and two-dimensional (below) binding modes of compound (**50b**) present at active site of C-terminal of human MGAM

Appendix 44 Three-dimensional (above) and two-dimensional (below) binding modes of compound (**50c**) present at active site of C-terminal of human MGAM

Appendix 45 Three-dimensional (above) and two-dimensional (below) binding modes of compound (**50d**) present at active site of C-terminal of human MGAM

Appendix 46 Three-dimensional (above) and two-dimensional (below) binding modes of compound (**50e**) present at active site of C-terminal of human MGAM

REKA BENTUK, SINTESIS, PENILAIAN BIOLOGI DAN KAJIAN PENDOKKAN MOLEKUL *ORTO*-KARBOKSAMIDO STILBENA SEBAGAI AGEN ANTI-DIABETIK DAN ANTI-PROLIFERASI

ABSTRAK

Sebelas *orto*-karboksamido stilbena (**50a-50k**) dengan jumlah hasil 63-83 % telah disintesis melalui kaedah penggandingan Heck yang telah diubahsuai. Sebatian yang disintesis telah dicirikan menggunakan spektroskopi FT-IR, NMR, dan HRMS. Kajian ini dimulakan dengan tindak balas Wittig oleh 3,5-dimetoksibenzaldehid (**45**) dan metiltrifenilphosphonium iodida untuk membentuk 3,5-dimetoksistirena (**46**), disusuli dengan tindakbalas Heck gandingan Pd(II) bersama derivatif amid (**49**) dalam kondisi bes untuk menghasilkan (*E*)-stilbena (**50a-50k**). Lima *orto*-karboksamido stilbena (**50a-50e**) kemudiannya diuji bagi kajian anti-diabetes ke atas enzim α-amilase dan α-glukosidase. Ujian antioksidan (penghapusan radikal bebas DPPH dan ujian FRAP) serta ujian MTT dilakukan untuk menyokong kajian anti-diabetes. Berdasarkan ujian ini, stilbena (**50d**) adalah perencat α-glukosidase yang paling kuat (IC_{50} = 6.62 ± 0.58 μM), manakala (**50e**) ialah perencat α-amilase yang paling kuat (IC_{50} = 9.03 ± 0.69 μM). (**50e**) menunjukkan aktiviti penghapusan radikal bebas DPPH tertinggi dengan IC_{50} terendah, 10.23 ± 0.33 μM. Pendokkan molekul (**50a-50e**) menunjukkan bahawa tenaga pengikat adalah diantara -7.9 hingga -9.0 kcal/mol untuk subunit terminal C bagi maltase glukoamilase manusia, ctMGAM (α-glukosidase) yang dikomplekskan dengan akarbosa (PDB ID: 3TOP) dan -7.2 hingga -8.5 kcal/mol untuk α-amilase yang dikomplekskan dengan nitrit dan akarbosa (PDB ID: 2QV4). Disamping itu, sitotoksisiti semua stilbena telah diuji terhadap empat sel kanser manusia (MCF-7, MDA-MB-231, MCF-7/TAMR-1, dan A549) bersama-sama

dengan sel normal manusia (MCF-10A dan BEAS-2B) menggunakan tamoxifen dan cisplatin sebagai kawalan positif. Selain itu, sitotoksisiti kesemua stilbene (**50a-50e**) diuji keatas empat sel kanser manusia (reseptor positif dan negatif estrogen manusia (MCF7 dan MDA-MB-231)), sel kanser payudara, sel tahanan tamoxifen (MCF-7/TAMR-1), dan sel adenokarsinoma paru-paru manusia (A549) bersama dengan sel payudara normal (MCF-10A) dan sel paru-paru normal (BEAS-2B) menggunakan tamoxifen dan cisplatin sebagai pemalar positif. Stilbena (**50d**), (**50f**), dan (**50g**) menunjukkan sitotoksisiti yang kuat terhadap sel A549 selepas 72 jam, dengan IC_{50} masing-masing: 10.4 µM, 6.47 µM, dan 8.99 µM. Kajian pendokkan molekul pada tapak pengikatan colchicine protein tubulin, α- dan *β*-subunit (PDB ID: 5LYJ) telah dilakukan untuk memahami interaksi reseptor-ligan (stilbena (**50d**), (**50f**), dan (**50g**)). Tenaga ikatan yang ditunjukkan oleh sebatian adalah masing-masing diantara -6.4 hingga -7.1 kcal/mol dan -6.3 hingga -6.6 kcal/mol untuk tapak pengikatan colchicine bagi protein tubulin subunit α- dan *β*.

DESIGN, SYNTHESIS, BIOLOGICAL EVALUATION, AND MOLECULAR DOCKING STUDIES OF *ORTHO*-CARBOXAMIDO STILBENES AS ANTI-DIABETIC AND ANTI-PROLIFERATIVE AGENTS

ABSTRACT

A total of eleven *ortho*-carboxamido stilbenes (**50a-50k**) in 63-83 % yield have been synthesized using our modified Heck coupling method, and characterized using FT-IR, NMR, and HRMS. The research started with the Wittig reaction of 3,5-dimethoxybenzaldehyde (**45**) and methyltriphenylphosphonium iodide to form 3,5-dimethoxystyrene (**46**) followed by the Heck reaction with amide derivatives (**49**) under basic conditions to provide the corresponding (*E*)-stilbene derivatives (**50a-50k**). Five *ortho*-carboxamido stilbenes (**50a**-**50e**) were subjected to anti-diabetic studies on α-amylase and α-glucosidase enzymes. The antioxidant assay (DPPH free radical scavenging and FRAP assays) as well as MTT assay were performed to support the anti-diabetic study. Based on this assay, stilbene (**50d**) was the most potent α-glucosidase inhibitor (IC_{50} = 6.62 ± 0.58 μM), while (**50e**) was the most potent α-amylase inhibitor (IC_{50} = 9.03 ± 0.69 μM). (**50e**) showed the highest DPPH free radical scavenging activity with the lowest IC_{50}, 10.23 ± 0.33 μM. The molecular docking of (**50a**-**50e**) shown that the binding energy were ranging from -7.9 to -9.0 kcal/mol for the C-terminal subunit of human maltase glucoamylase, ctMGAM (α-glucosidase) complexed with acarbose (PDB ID: 3TOP) and -7.2 to -8.5 kcal/mol for α-amylase complexed with nitrite and acarbose (PDB ID: 2QV4). In addition, the cytotoxicity of all stilbenes was tested against four human cancer cell lines (human estrogen receptor positive (MCF-7) and negative (MDA-MB-231) breast cancer cell lines, tamoxifen-resistant cell line (MCF-7/TAMR-1), and human lung adenocarcinoma cell line

(A549) together with normal breast cells (MCF-10A) and normal lung cells (BEAS-2B) using tamoxifen and cisplatin as a positive control. Stilbene (**50d**), (**50f**), and (**50g**) showed strong cytotoxicity to A549 cells after 72 hours, with IC_{50}: 10.4 ± 1.49 µM, 6.5 ± 1.14 µM, and 8.8 ± 0.81 µM, respectively. The molecular docking studies on the colchicine binding site of tubulin protein, α- and β-subunits (PDB ID: 5LYJ) were done to understand the ligand-receptor interactions on stilbene (**50d**), (**50f**), and (**50g**). The binding energy were ranging from -6.4 to -7.1 kcal/mol and -6.3 to -6.6 kcal/mol for the colchicine binding site of the tubulin protein, α- and *β*-subunits respectively.

CHAPTER 1

INTRODUCTION

1.1 Overview

Advances in synthetic chemistry have paved the way for researchers in this area with multiple basic and applied research applications of stilbene. The unique chemistry of two aromatics rings, joined by an ethylene bridge forming a C6–C2–C6 chain, has sparked various constructions. The aromatic rings could be substituted by different functional groups such as hydroxyl, methoxyl, prenyl, or geranyl (Pecyna et al., 2020a). The double bond of the ethylene bridge allows stilbenes to exist in two isomeric forms: (*E*)-stilbene (*trans*-stilbene) (**1**) and (*Z*)-stilbene (*cis*-stilbene) (**2**) (Figure 1.1) (Rivière et al., 2012). The different conformations come with different characteristics, represented in stilbenes by the dramatic difference in melting point. The *trans*-isomer has been reported as the most stable stilbene from the steric point of view (Latva-Mäenpää et al., 2021). The sterically hindered *cis*-stilbene is less stable, with a melting point of 6 ºC, while *trans*-stilbene has a melting point of 125 ºC (Likhtenshtein, 2012).

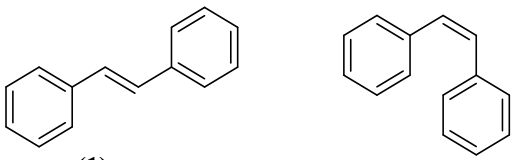

Figure 1.1 The chemical structures of stilbenes isomers

From literature, *trans*-stilbene could isomerize to *cis*-stilbene under the influence of light, and the reverse path can be stimulated by heating or under UV-light (Görner & Kuhn, 1994). Resveratrol (**3**), piceatannol (**4**), and oxyresveratrol (**5**) are

recognized to be representatives of *trans*-polyphenolic stilbenes (Figure1.2) (Digafie et al., 2021).

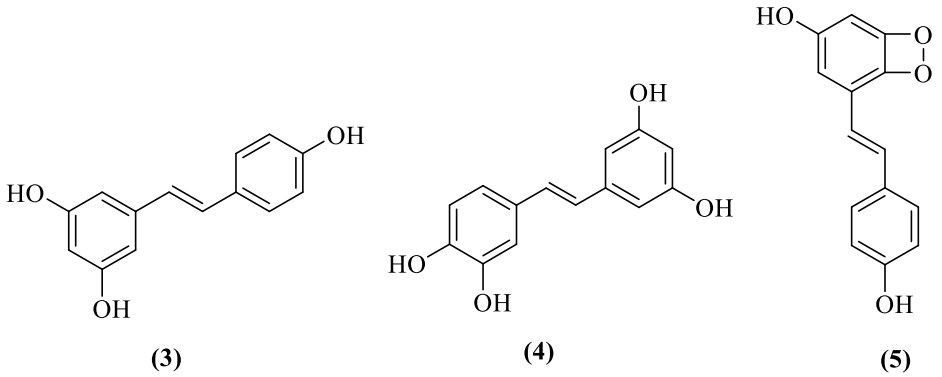

Figure 1.2 The chemical structures of *trans*-polyphenolic stilbenes

Apart from the numerous natural stilbenes, including hydroxylated (Pezzuto, 2019; Piotrowska et al., 2012), methoxylated (Lin et al., 2020; Sherbet, 2020), glycosylated (S. G. Li et al., 2019), and prenylated (Yan et al., 2019) derivatives, various chemical modifications of natural stilbenes have been designed to increase the potency, selectivity, and pharmacokinetic properties (Reinisalo et al., 2015).

Over a thousand natural stilbenes have been described in the literature, and among them, *trans*-resveratrol is undoubtedly the most popular and broadly studied for its health benefits (Pezzuto, 2019). Stilbenes have exhibited to hold a great range of biological activities, potentially beneficial for human health, such as neuroprotective, anti-oxidant, and anti-tumour effects (Weiskirchen and Weiskirchen 2016), as well as anti-tobacco mosaic virus, and anti-phytopathogenic fungus agents (Song et al., 2021).

Previously nineteen *ortho*-carboxamido stilbenes have been synthesized, integrated with the amide moiety, and portrayed an excellent biological activity for their cytotoxicity against six human cell lines: colon cancer (HT-29), estrogen-

sensitive breast cancer (MCF-7), estrogen insensitive breast cancer (MDA-MB-231), prostate cancer (DU-145), pancreatic cancer (BxPC-3) and normal pancreatic cells (hTERT-HPNE) (Azmi et al. 2013).

As part of continuing studies, a series of *ortho*-carboxamido stilbene derivatives originating from the Heck coupling reaction were synthesized. This coupling reaction offers an easy and direct approach toward *ortho*-carboxamido stilbene with styrene and iodocarboxamido as the starting materials. This study marked the first report for biological (anti-diabetic) activity on *ortho*-carboxamidostilbenes, where no previous report was recorded.

1.2 Problem Statement

Non-communicable diseases (NCDs) are also termed chronic diseases of long duration and generally slow progression due to genetic, physiological, environmental, and behavioural features. The tremendous burden of this rising threat stood by the four most common NCDs: cardiovascular diseases (such as heart attacks and stroke), cancers, chronic respiratory diseases (such as chronic obstructive pulmonary disease and asthma), and diabetes. NCDs kill 41 million people each year, equivalent to over 7 out of 10 deaths worldwide (World Health Organization, 2020) (Figure 1.3). Therefore, to address this gap, a new cost effective and straight forward synthesis steps of anti-diabetic and anti-proliferative agents need to be design for the treatment of diabetes and cancer (Rambaran, 2020) (Hua et al., 2018).

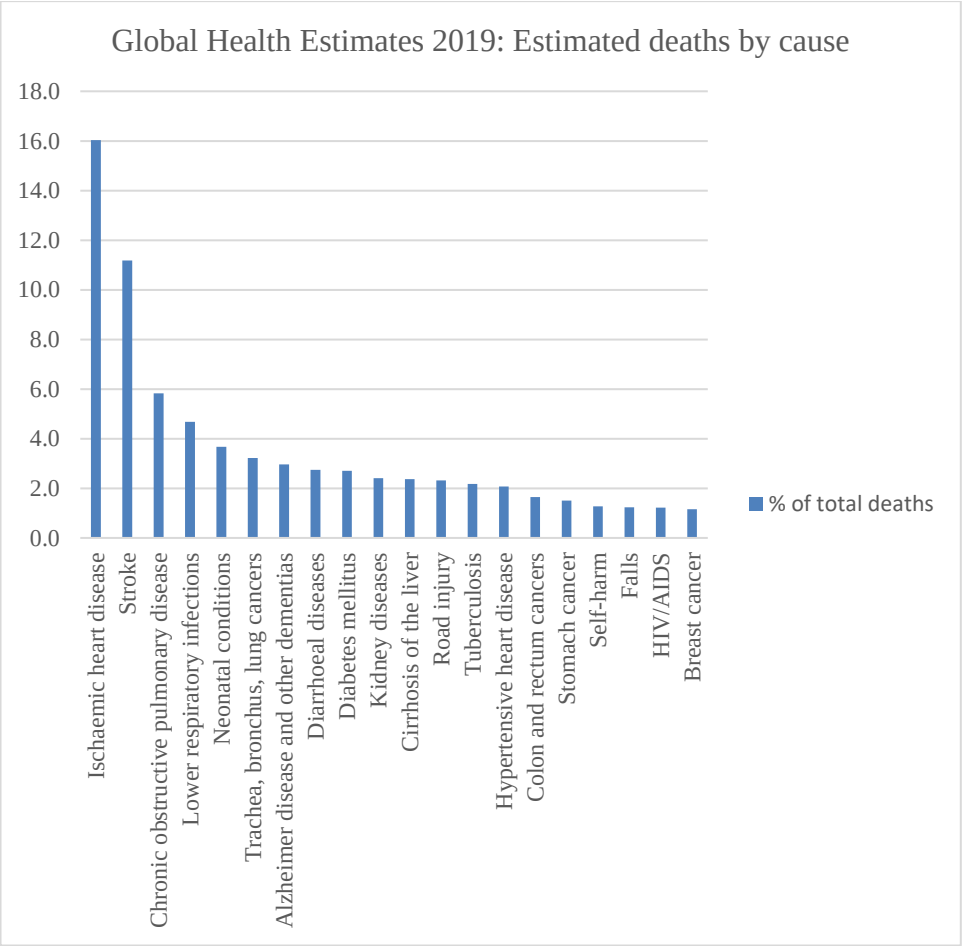

Figure 1.3 The bar chart of Global Health Estimates 2019 (World Health Organization, 2020)

Inspired by the previously reported biological potency of *ortho*-carboxamido stilbenes, this research focused on the synthesis of new *ortho*-carboxamido stilbenes via Heck coupling and its biological evaluation as anti-diabetic and anti-proliferative agents. Based on their biological activity, *in silico* molecular docking helps to validate the *in vitro* results. Assessing the therapeutic potential of *ortho*-carboxamido stilbenes could give us insight into how best these compounds can be employed to treat dreaded diseases.

1.3 Research Objectives

Literature survey indicated that there is little work on the anti-diabetic and anti-proliferative properties of *ortho*-carboxamido stilbenes. Considering the above, the objectives have been addressed as follows:

1. To synthesize and characterize a series of *ortho*-carboxamido stilbenes with different amide moieties *via* the Heck coupling method.

2. To determine the anti-proliferative activity of the synthesized analogs against cancer cell lines.

3. To evaluate the effect of different stilbene derivatives on the anti-diabetic activity on α-amylase and α-glucosidase enzymes.

4. To perform *in silico* molecular docking studies to validate the *in vitro* results of their anti-proliferative and anti-diabetic activities.

1.4 Scope of Research

The research involved synthesizing new *ortho*-carboxamido stilbenes and characterization work methods NMR, FT-IR, and HRMS. Samples for anti-proliferative studies were prepared and submitted to Advanced Medical and Dental Institute (AMDI), USM. The samples were also tested for anti-diabetic studies at the School of Industrial Technology, USM. The *in silico* molecular docking screening was done at the School of Chemical Sciences, USM using the software required.

CHAPTER 2

LITERATURE REVIEW

2.1 Stilbene Compound

Resveratrol (3,4',5-trihydroxystilbene) (**3**) is a pleiotropic phytochemical belonging to a class of polyphenolic compounds called stilbenes. Stilbenes are the family of bioactive compounds of natural defence phenolics in many plants species, which are abundant in grapes, berries, and conifer bark waste (Reinisalo et al., 2015b). Polyphenols have become significant as natural antioxidants to prevent and treat cancer (Younas et al., 2018) and inflammatory, cardiovascular, and neurodegenerative diseases (Quideau et al., 2011). Polyphenols can be classified generally into four types based on the number of phenol rings present and the structural components that connect to those rings; flavonoids (**6**), lignans (**7**), coumarins (**8**), stilbenes (**9**), and phenolic acids (**10**) (Durazzo et al., 2019)(Figure. 2.1).

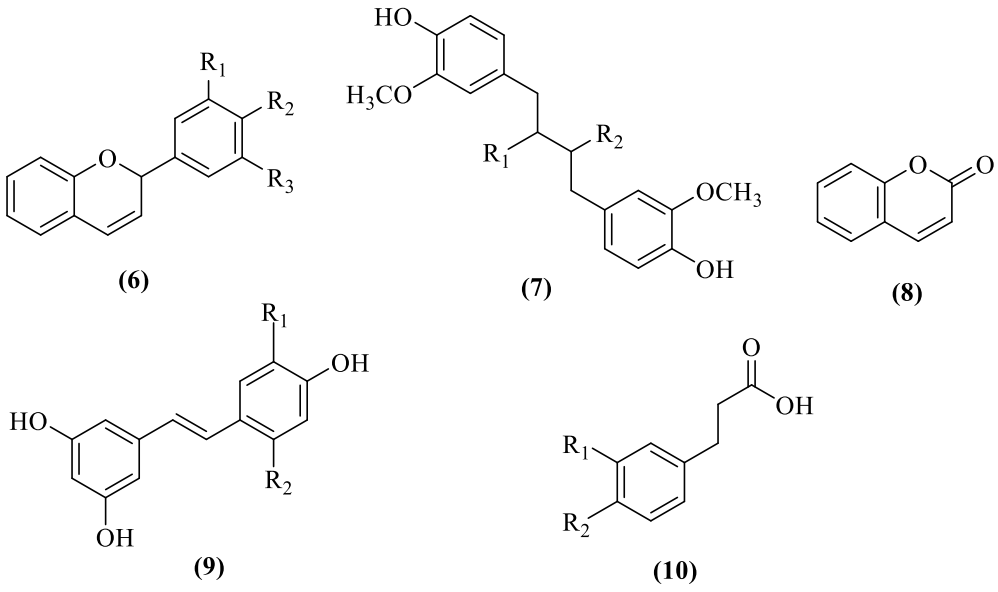

Figure 2.1 Some examples of plant polyphenols

Both flavonoids and stilbenes are derived from the phenylpropanoid metabolism, however flavonoids are ubiquitous in plants, whereas stilbenes are specific to certain plant families (Almagro et al. 2013). In addition, hydroxyl groups permit polyphenols to associate with proteins and other nutrients (Shahidi et. al 2015).

The biosynthesis of resveratrol (**3**) involved four steps from phenylalanine (**11**) as starting molecule (Scheme 2.1). The immediate precursors of resveratrol are *para*-coumaroyl CoA (**14**) and malonyl CoA (**15**) in a molar ratio of 1:3. By losing its amino group through oxidative deamination catalyzed by a phenylalanine ammonia lyase, phenylalanine (**11**) is converted to cinnamic acid (**12**). Cinnamate-4-hydroxylase then catalyzes cinnamic acid conversion (**12**) to *para*-coumaric acid (**13**). In the final step, *para*-coumaroyl CoA (**14**) is generated with the help of coumaroyl-CoA ligase, which also results in the condensation of three molecules of malonyl CoA (**15**), which then produces the resveratrol (**3**) (Emiliani et al., 2009) A transcriptional factor, Myb14, has been found to regulate the expression of the enzyme stilbene synthase (Crupi et al. 2013).

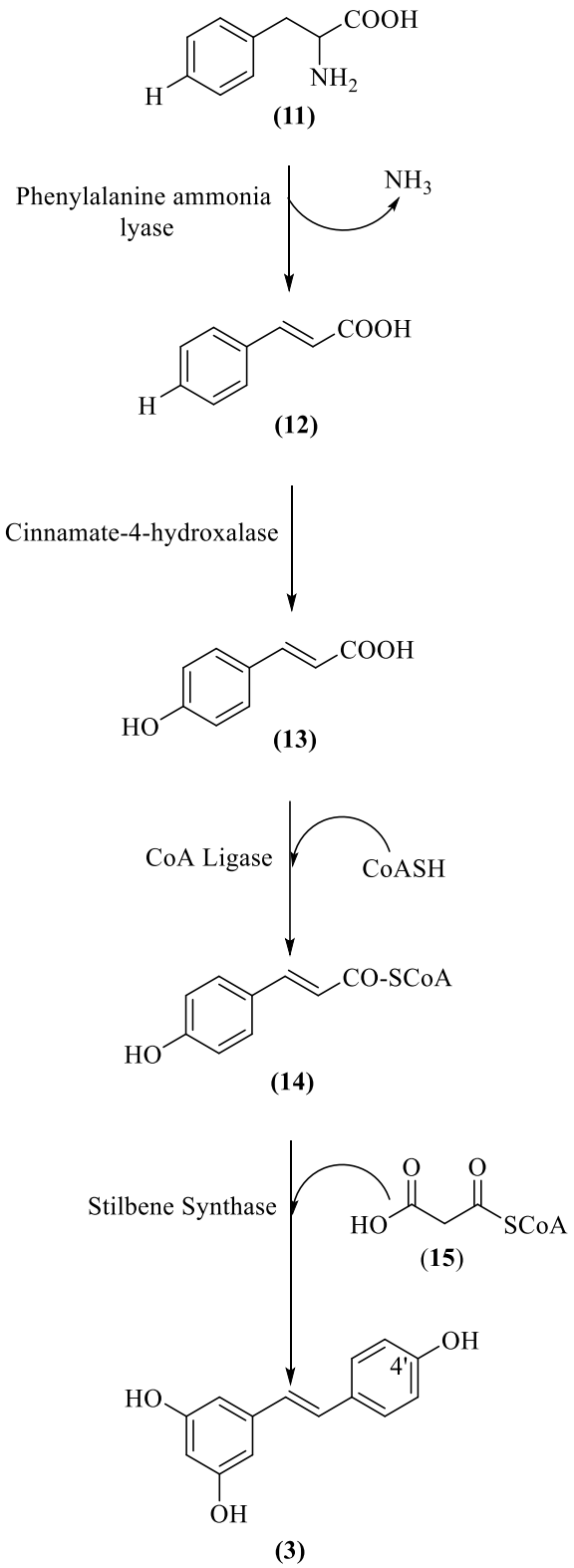

Scheme 2.1 Biosynthesis of resveratrol *via* phenylalanine (Shrestha et al., 2019)

2.2 Stilbene Synthesis

Stilbene synthesis featuring cross-coupling of arenes and styrenes has attracted substantial attention in organic synthesis (Mochida et al., 2010). The strategies in the synthesis of stilbene mainly involve palladium-mediated coupling reactions. Heck and Suzuki reactions stand out for their synthetic versatility and efficiency (Ferré-Filmon et al., 2004). In this research, the Heck coupling reaction will be adapted due to the reaction's adaptability and expandability (Beletskaya and Cheprakov 2000), minimal use of catalyst and ligand, direct synthesis step, and well-established reaction mechanism (Kee et al. 2010).

The Heck cross-coupling reaction is a palladium-catalyzed coupling of aryl halide (substituted benzene) with an alkene (commonly propene) to form a more highly substituted alkene with a new C–C bond (**16**) (Scheme 2.2). The aryl replaces one H atom of the alkene. Palladium (II) acetate, $Pd(OAc)_2$ in the presence of a triarylphosphine ($P(o\text{-tolyl})_3$) will act as the catalyst, and in most cases, a stoichiometric amount of base such as triethylamine, Et_3N (Smith, 2011, p. 1009). The reactivity of aryl halide governs the rate-determining steps; it decreases in the order ArI > ArBr >> ArCl (Vikse et al., 2013).

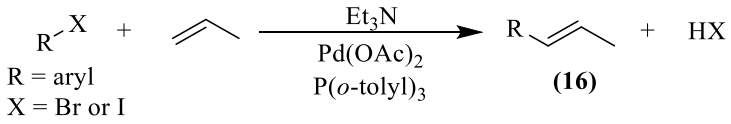

Scheme 2.2 General scheme for Heck reaction

Alkene used can either be ethylene or a monosubstituted alkene (Smith, 2011, p. 1009). Based on the Scheme 2.3 below, an aryl halide (**17**) is used to react with styrene (**18**) to yield stable (*E*)-stilbene (**1**).

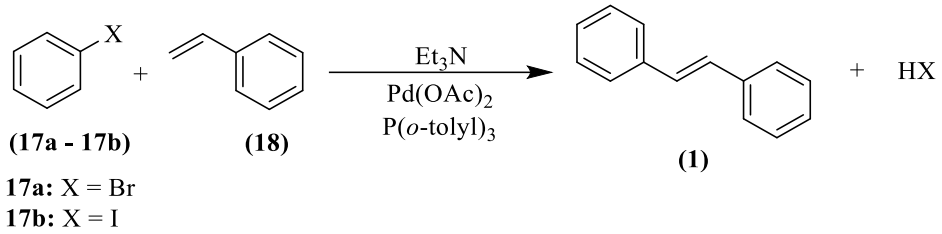

Scheme 2.3 Synthesis of stilbene (**1**) from Heck reaction

Karthikeyen and co-workers have introduced palladium functionalized 1-glycyl-3-methyl imidazolium chloride complex, [Gmim]Cl–Pd (II) (**19**) as a novel heterogeneous catalyst for Heck–Mizoroki reaction with Et_3N under solvent-free condition via green approach. Figure 2.2 showned that the structure of tetra-coordinated palladium complex (**19**) which was prepared by reacting $PdCl_2$ with 1-glycyl-3-methyl imidazolium chloride, and its catalytic function was invented for the C-C bond formation (Karthikeyan et al., 2012).

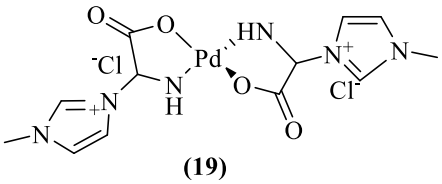

Figure 2.2 Structure of compound (**19)**

Aryl bromides or chlorides (**20)** were reacted efficiently with styrene (**21)** at ambient temperature in the presence of the catalyst (**19)** based on the Scheme 2.4. Aromatic halides with a withdrawing group were more reactive than those electrons donating group (Bariwal et al., 2018). This catalytic system has synthesized a novel palladium complex (**19**); its catalytic activity was tested in Heck reaction with a sufficient amount of 0.1 mmol of catalyst to furnish the *trans*-stilbenes (**22**) with

excellent yields of targeted stilbenes (up to 96%). (4) The catalyst can be readily recovered and reused without significant loss of its activity (Karthikeyan et al., 2012).

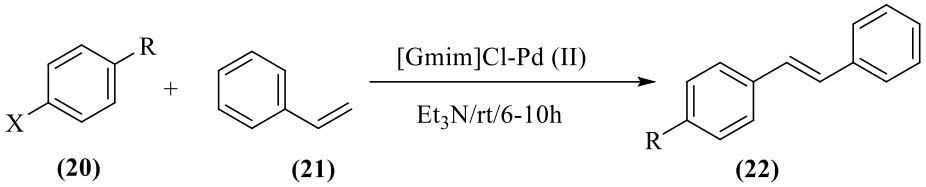

(20) **(21)** **(22)**

20a: R= - X= Cl
20b: R= NO_2 X= Cl
20c: R= CH_3 X= Cl
20d: R= - X= Br
20e: R= CH_3 X= Br
20f: R= OCH_3 X= Br
20g: R= Cl X= Br
20h: R= N X= Br

22a: R= -
22b: R= NO_2
22c: R= CH_3
22d: R= -
22e: R= CH_3
22f: R= OCH_3
22g: R= Cl
22h: R= N

Scheme 2.4 Heck–Mizoroki coupling of an aryl halide (**20**) with styrene (**21**) in the presence of catalyst [Gmim]Cl–Pd (II) and Et_3N as a base

Since it is critical to design a rewarding catalytic system that achieves excellent selectivity and high activity to aryl chlorides, Ataei et al. have developed another palladium catalytic system, 2,6-bis(diphenylphosphino) pyridine (**23**). Compound (**23**) in Figure 2.3 can catalyze the arylation of reaction between styrene and aryl chlorides or bromides containing either electron-rich or electron-withdrawing functional groups has shown high selectivity for the *trans*-configured product (Ataei et al., 2013).

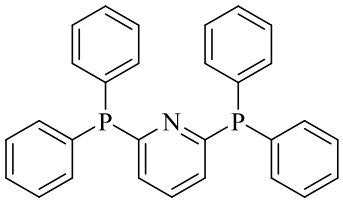

(23)

Figure 2.3 Structure of compound (**23**)

The combination of (**23)** and dimethylacetamide (DMAc) as the solvent, K_2CO_3 as the base, and 3 mmol tetrabutylammonium bromide (TBAB) as an additive

yielded 92% of (**24)** (Scheme 2.5). The rigidity and strong donor properties of ligand (**23**) result in a highly active and selective catalyst for the Heck reaction at minimal Pd loading (Ataei et al., 2013).

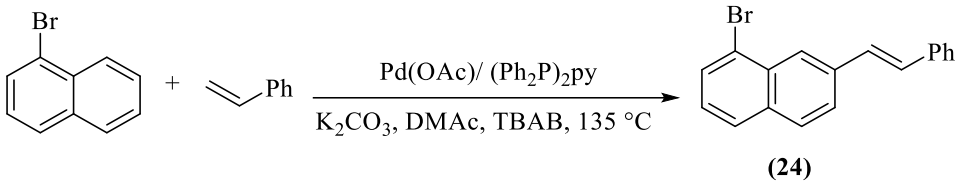

Scheme 2.5 Heck reaction of aryl bromides with styrene in the presence of K_2CO_3 base and TBAB

The synthesis of stilbenes (**27**) through microwave-assisted Heck coupling reaction of C-aryl glycosides (**25**) and styrenes (**26**) has been developed by Kumar research team (Scheme 2.6). The Pd-catalyzed Heck coupling reaction was successfully applied to various functionalized C-glycosyl aryl iodides and various substituted styrenes to deliver several C-glycoside *trans*-stilbenes with high selectivity and with a yield range from 60 % to 65% (Kumar Ponnapalli et al., 2017).

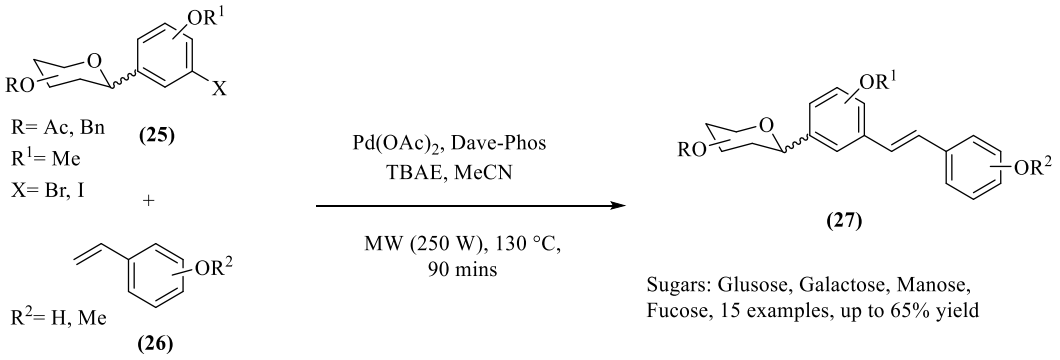

Scheme 2.6 Synthesis of *trans*-stilbene C-glycosides (**27**) by a microwave-assisted Heck reaction

Among all the synthesized *trans*-stilbene C-glycosides derivatives in Scheme 2.6, compound (**28**) (Figure 2.4) showed the most significant IC_{50} value for Sodium-glucose cotransporter 2 (SGLT-2) inhibitor of 12.2 ± 4.6 µM. Stilbenoids containing

glucose and a free hydroxyl group at the 4′ positions of the stilbene core showed promising efficacy, emphasizing the need for one or more free hydroxyl substituents on the stilbene core when designing the next-generation SGLT-2 inhibitor (Kumar Ponnapalli et al., 2017).

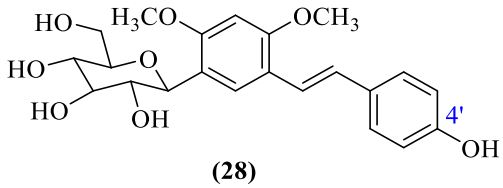

(28)

Figure 2.4 Structure of compound (**28**)

2.3 Role of Stilbenes in the Prevention of Cancer

Cancer has emerged as a major public health concern around the world. Its annual and global incidence is in the millions, particularly in developed countries, resulting in well over 6 million yearly fatality rates (World Health Organization 2020). Chemo prevention, in combination with anti-cancer treatment, is essential to reduce morbidity and mortality. Stilbene-based compounds have attracted the attention of many researchers over the years due to their wide-ranging biological activities. The accumulating data have demonstrated potential anticancer activity at the initiation, promotion, and progression stages (Jang et al. 1997). In fact, structure–activity studies have discovered essential elements of the stilbenic backbone that are required for specific effects. The 4-hydroxy group in the *trans* conformation on the 4- and 4′-positions of the stilbenic backbone (**3**) has been found crucial for resveratrol's antiproliferative effect (Stivala et al., 2001). Thus, new stilbene derivatives are designed and synthesized so that the new compounds therapeutic activities are superior to the parent compound.

In the previous study by the Haitao research group, pentamethoxy-*trans*-stilbene (PMS) (**29**) (Figure 2.5) was discovered to be a potent apoptosis-inducing agent against human colon cancer cells via targeting microtubules and silenced tumour growth in a colon cancer xenograft model. However, their poor water solubility has limited the development of polymethoxylated stilbenes as therapeutic agents. To improve such pharmacological properties, further rational design is considered necessary, and the introduction of the phosphate ester moiety or the boronic acid group is suggested (H. Li et al., 2010)

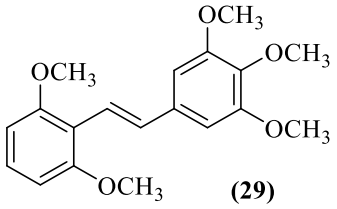

(29)

Figure 2.5 Structure of compound (**29**)

Trimethoxyl stilbene (TMS) (**30**) is a derivative of resveratrol (**3**) that displayed inhibition on a variety of tumour types (Figure 2.6) as reported by Liu et al. TMS inhibited A549 cell proliferation with an IC_{50} of 8.6 μmol/L and subsequently decreased both the number and size of the A549 cell colonies formed in a concentration-dependent manner (Liu et al., 2011). Interestingly, TMS was more potent compared to the parent compound (**3**) in inhibiting two human breast adenocarcinoma and one hepatoma cell line, but the IC_{50} required was >150 μM (Alex et al., 2010).

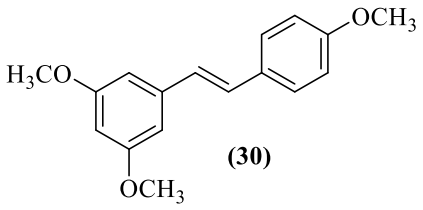

Figure 2.6 Structure of compound (**30**)

Mikstacka's research team synthesized seven *trans*-stilbene derivatives with a 4-methylthio substituent group to test for inhibitory properties towards cytochrome P450 isozymes CYP1A1, CYP1B1 and CYP1A2. (Mikstacka et al., 2014). Based on Figure 2.7, compound (**31**) inhibited CYP1A1 and CYP1B1 cell lines but did display a very low inhibition affinity towards the CYP1A2 cell line, having IC_{50} values of 0.9, 1.0, and > 50 µM, respectively. Compound (**32**) was revealed to be an effective inhibitor of all CYP1 cell lines, having IC_{50} values of 3.6, 2.6, and 7.0 µM for CYP1A1, CYP1B1, and CYP1A2 cell lines, respectively (Mikstacka et al., 2012).

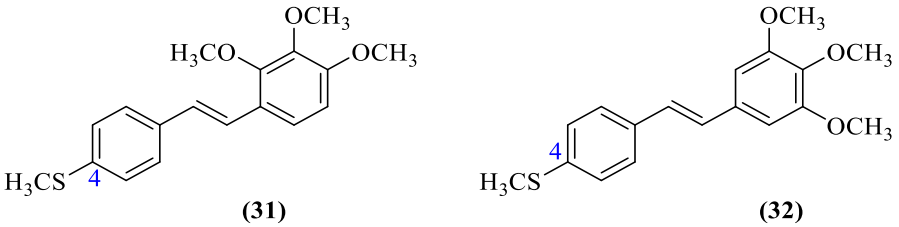

Figure 2.7 Structure of 4-methylsubstituted *trans*-stilbene with significant inhibitory action toward three cancer cell lines

Azmi and co-workers synthesized 19 resveratrol analogs with different amide moieties via the Heck reaction and tested them for toxicity against various cell lines, including human pancreatic cancer cell line (BxPC-3), human prostate cancer cell lines (DU-145), human colon cancer cell line (HT-29), human pancreatic nestin expressing cells (hTERT-HPNE), human estrogen receptor-positive breast cancer cell line (MCF-

7), and human estrogen receptor-negative breast cancer cell line (MDA-MB-231) cell lines (Azmi et al., 2013). None of the 19 synthesized stilbenes demonstrated cytotoxicity towards hTERT-HPNE and MDA-MB-231 (Azmi et al., 2013). Compound (**33**) demonstrated excellent cytotoxicity towards the HT-29 cancer cell line with an IC_{50} value of 7.51 ± 0.53 µM (Figure 2.8). Compound (**34**) exhibited cytotoxicity towards the DU-145 cancer cell line with an IC_{50} value of 16.68 ± 1.86 µM. At the same time, compound (**35**) demonstrated excellent cytotoxicity towards the MCF-7 cancer cell line with an IC_{50} value of 21.24 ± 1.01 µM, whereas compound (**36**) exhibited average cytotoxicity towards the BxPC-3 cancer cell line with an IC_{50} value of 66.30 ± 1.14 µM (Azmi et al., 2013).

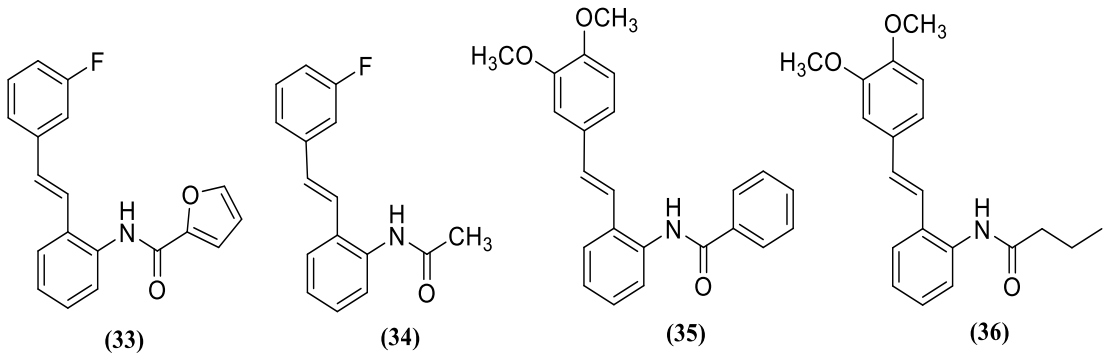

Figure 2.8 Structure of amide substituted resveratrol with potent cytotoxicity towards the respective cancer cell lines

Mulakayala and colleagues further investigated the anti-proliferative activity of stilbene (**37**) and (**38**) (Scheme 2.7) on the U937 cancer cell line, together with resveratrol (**3**) acting as a comparison for the two stilbene derivatives (Mulakayala et al., 2013). The activity was tested at four concentrations: 1, 3, 5, and 10 µM. Stilbene (**37**) had the most potent anti-proliferative activity (highest percentage of cell death at 10 µM), three times more than that of resveratrol (**3**) (Mulakayala et al., 2013). The IC_{50} values calculated for resveratrol (**3**), stilbenes (**37**), and (**38**) are 32.01 µM, 10.372

μM, and 13.372 μM, respectively. Stilbenes (**37**) and (**38**), might have displayed higher pharmaceutical activity and bioavailability than their parental molecule resveratrol (**3**), due to the capping of hydroxyl groups (Pecyna et al., 2020).

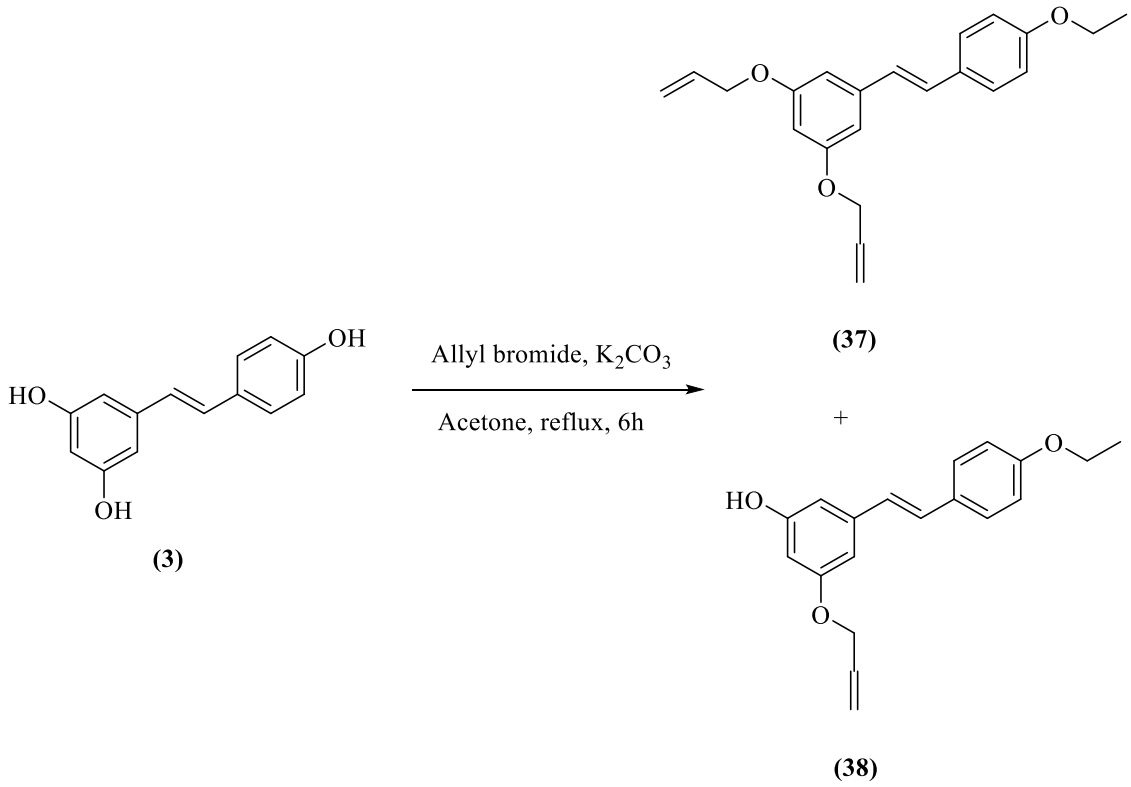

Scheme 2.7 Structure of two stilbene derivatives (**37**) and (**38**) that showed potent antiproliferative activity on U937 cancer cell line

Yousuf's research team utilized nine twin-chain cationic lipid conjugated, methoxy-enriched stilbene derivatives to overcome poor pharmacokinetic properties and non-selectivity of stilbene-based compounds towards cancer and non-cancer cogency (Yousuf et al., 2020). Stilbene (**39**) (Figure 2.9) portrayed a beneficial effect among all tested molecules for cervical cancer cells with an IC_{50} value of 4.61 μM. The studies have supported that by increasing number of methoxy groups and long-chain lengths; the selectivity will improve with lesser IC_{50} (Menezes et al., 2011).

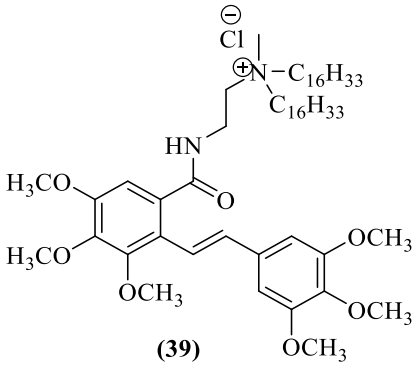

(39)

Figure 2.9 Structure of modified stilbene (**39**) with the most proficient anti-cervical cancer agent with the self-aggregation property

By referring to the statements described above, it was evident that resveratrol (**3**) has found a wide-ranging application in the medical field by inhibiting the proliferation and induction of apoptosis. However, resveratrol (**3**) has low bioavailability and requires a high dose to induce apoptosis in cancer cells (Walle et al., 2004). This drawback gives rise to improving its pharmacokinetic properties, thus enhancing the respective anticancer activity.

2.3.1 Tubulin protein in cancer

Natural products and their derivatives, including paclitaxel, docetaxel, vinblastine, vincristine, vinorelbine, vindesine, and ixabepilone, have proven to be highly effective as microtubule-targeting anticancer drugs (Miller et al., 2018). Stilbene that targets microtubules and disrupts the normal function of the mitotic spindle fibers has proven to be one of the best classes of cancer chemotherapeutic drugs available in clinics to date (Mukhtar et al., 2014b). Combretastatin is a tubulin polymerization inhibitor that occurs naturally. Tubulin polymerizes to form microtubules, making it an attractive target for developing anticancer agents (Mikstacka et al., 2013). Tubulin microtubules are composed of α-tubulin and β-

tubulin heterodimers, as shown in Figure 2.10. α-Tubulin and *β*-tubulin are dynamic polymers in eukaryotic cells and play vital roles in cell division, motility, transport, and signaling (Horio et al., 2014). They are formed during the polymerization of α-tubulin and *β*-tubulin dimers. Any compound that interferes with microtubule kinetics is known as a potential antimitotic drug due to the irreplaceable role of microtubules in cellular life activities (van Vuuren et al., 2015). Even minor alterations of microtubule dynamics can engage the spindle checkpoint, arresting cell cycle progression at mitosis and leading to cell death (Mukhtar et al., 2014). Thus, antimitotic drugs function in a cell-cycle-dependent manner.

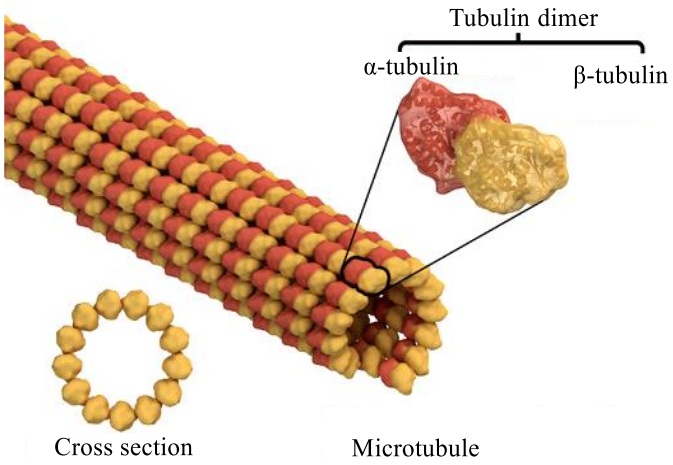

Figure 2.10 Structure of tubulin dimer and its cross-section

Figure 2.11 shows the structure of combretastatin A-4(CA-4) (**40**), a methoxylated and hydroxylated substituted stilbene with cytotoxic potential that inhibits tubulin polymerization by binding to the colchicine site (Shan et al., 2011). Modifications to the CA-4 structure have resulted in many novel CA-4 derivatives as potent tubulin inhibitors and high cytotoxic anticancer medicines (Duan et al., 2016). Molecules in the combretastatin family have three structural properties in common: a

trimethoxy A ring, a B-ring containing substituents often at C3′ and C4′, and an ethene bridge between the two rings which gives structural rigidity (Shan et al., 2011).

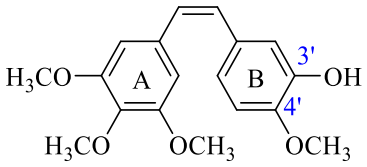

(40)

Figure 2.11 Structure of Combretastatin A-4 (CA-4)

Jadala's research team has synthesized a new series of CA-4 linked sulfonyl piperazine hybrids and further evaluated them for their *in vitro* anti-proliferative activity on a panel of human cancer cell lines (Jadala et al., 2019). The *in vitro* screening signifies that the most active compound (**41**) (Figure 2.12) displayed an extensive range of activity on all the tested cancer cell lines with an IC_{50} value of 0.36±0.02 μM on A549 cells. (Jadala et al., 2019). The flow cytometric analysis indicated the cell cycle arrest in A549 cells at the G2/M phase. In addition, compound (**41**) efficiently inhibited tubulin polymerization with an IC_{50} value of 5.24±0.06 μM, and *in silico* studies also declared that compound (**41**) binds into the combretastatin-binding space on the colchicine binding site of the tubulin.

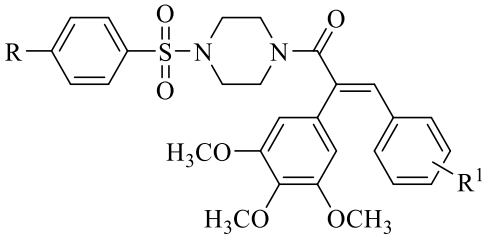

R = -H, -CH_3, -OCH_3, -$C(CH_3)_3$, -Cl

R^1 = 2-OEt, 4-OCH_3, 4-CH_3, 4-Cl, 4-F, 4-CF_3

(41)

Figure 2.12 Structure of compound (**41**)

The structure-activity relationship (SARs) has concluded that 4-chloro substitution on C4 of sulfonamide ring was responsible for the compound to show cytotoxicity. The compounds are listed in descending order of cytotoxicity based on sulfonamide and CA-4 ring substitutions as Cl–Cl > Cl–CH_3 > Cl–OCH_3 (Jadala et al., 2019).

The recent findings from Egharevba research team on the sulfonyl analogs of CA-4 showed moderate to good activity and non were cytotoxic towards normal healthy cell lines (HEK 293) except compound (**42**) (Figure 2.13), which showed some level of cytotoxicity. The observed results from both *in silico* and *in vitro* studies show that the compounds constitute a potential lead source based on the anticancer activity against four cancer cell lines, MDA-MB 231 (breast cancer), HeLa (cervical cancer), A549 (lung cancer), and IMR-32 (neuroblast cancer). As a result of positive induction, molecules with electron donating substituent(s) outperformed those with electron withdrawing substituent(s) (Egharevba et al., 2022). More halogen substituents at different positions (and perhaps on the other aromatic ring) to investigate if there would be an improvement in the anticancer profiles of the optimized compounds.

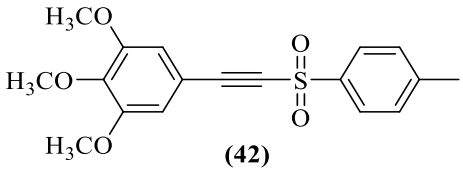

(42)

Figure 2.13 Structure of compound (**42)**

2.4 Role of stilbene as enzyme inhibitors of hyperglycemic enzymes and the enzymatic pathways

Stilbenes have been reported to reduce the risk against various chronic diseases, including cardiovascular disease, malignancies of various sorts, neurological diseases, and insulin resistance (IR) (Kershaw and Kim 2017). According to Szkudelska et al., resveratrol (**3**) has a calorie constraint mimetic effect, which can inhibit some diseases of aging, such as insulin resistance and type 2 diabetes mellitus (Szkudelska et al., 2010). A recent review has shown that resveratrol (**3**) could be used to treat non-alcoholic fatty liver disease because of its anti-inflammatory, antioxidant, and calorie-restricting properties (Izzo et al., 2021).

The study from Wang's group has presented the discovery of a rare stilbene sestermer (**43**) as shown in Figure 2.14. From the biological evaluation, stilbene sestermer increased the glucose consumption in HepG2 cells equivalent to the positive control rosiglitazone and markedly inhibited the activity of α-glucosidase (F. Wang et al., 2021).

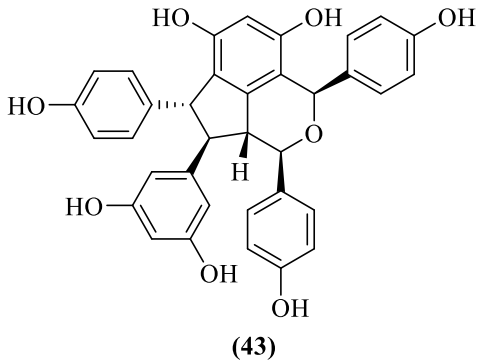

(43)

Figure 2.14 Structure of compound (**43**)

The modifications of the stilbene core by Dutra and co-workers have highlighted compound (**44**) (Figure 2.15) as a promising prototype for developing novel candidate to treat dyslipidemia and diabetes mellitus (Dutra et al., 2022).

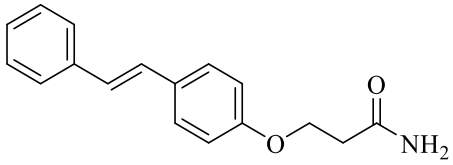

(44)

Figure 2.15 Structure of compound (**44**)

In vitro and *in vivo* assays revealed that the lead compound (**44**) removed ^{14}C-cholesterol from the foam cells through apolipoprotein A-I and High-Density Lipoprotein-2(HDL-2). In the high-fat diet-induced obesity mouse model, the oral administration of compound (**44)** increased the HDL levels, paraoxonase-1 activity, and insulin sensitivity, as well as decreased the glucose levels. Moreover, the adipogenesis pathway and triglyceride accumulation gives slightly changes in the adipocyte cells upon treatment with compound (**44**), without affecting the body weight and adipose tissue in obese mice (Dutra et al., 2022).

2.4.1 Overview of Diabetes Mellitus (DM)

Diabetes mellitus (DM) has become apparent as one of the most serious and common chronic diseases of our times, causing life threatening, disabling, and costly complications, as well as reducing life expectancy (Heald et al., 2020). DM is a chronic metabolic syndrome due to abnormally high blood glucose levels. Absolute or relative lack of insulin caused by pancreatic β-cell dysfunction, insulin resistance, or both is the main reason for high blood sugar levels (hyperglycemia) (Association, 2013).

Insulin serves as a hormone that transports glucose into the blood cell. When insulin production is dropped, cellular glucose uptake will be disrupted, resulting in high blood sugar levels hyperglycemia (Shoaib et al., 2018). There are few distinct classes of drugs that potentially cure DM. Sulfonylureas have been extensively used for treatment of DM (Bhatt et al., 2012). Consumption of this class of drugs among people with obesity will cause an adverse reaction in weight gain (Phung et al., 2010). The continuous use of some antidiabetic drugs is linked with various side effects such as gastrointestinal symptoms (Chaudhury et al., 2017). There is a demand for hyperglycaemia inhibitors which have no undesired side effects. Thus, it seems clear that new treatments are immediately required to properly manage the different forms of DM.

2.4.2 Target protein for diabetes

α-Amylase is a family of endoamylases, the vital enzyme found in the pancreatic juice and saliva which take part in carbohydrates breakdown and the glucose metabolism process into absorbable molecules (Brayer et al., 1995). The α-amylase contribution is a prerequisite for initiating this process as it serves as the significant digestive enzyme in carbohydrates breakdown and helps in intestinal absorption (Peyrot des Gachons & Breslin, 2016). The inhibitory mechanism of protein to α-amylase happens by promptly blocking the active centers of several subsites of the enzyme (Payan, 2004).

α-Glucosidase is a carbohydrate-hydrolase that releases α-glucose to catalyze the hydrolysis of disaccharides such as maltose and sucrose into simpler monosaccharides (glucose). The substrate selectivity of the α -glucosidase enzyme is because of sub-site attractions of the enzyme's active site. Similar to α-amylase, α-